Engineering Analysis with Boundary Elements 93 (2018) 72–82

Contents lists available at ScienceDirect

Engineering Analysis with Boundary Elements

journal homepage: www.elsevier.com/locate/enganabound

The method of transformed angular basis function for solving the Laplace equation

Xinxiang Li [a], Jaeyoun Oh [b], Yong Wang [c], Huiqing Zhu [b,*]

[a] Department of Mathematics, College of Science, Shanghai University, Shanghai 200444, China
[b] Department of Mathematics, University of Southern Mississippi, Hattiesburg, MS 39406, USA
[c] Department of Obstetrics and Gynecology, Radiology, Biomedical Engineering, Washington University, St. Louis, MO 63130, USA

ARTICLE INFO

MSC:
65N22
65N35

Keywords:
Method of fundamental solution
Angular basis functions
Transformed angular basis functions

ABSTRACT

In this paper, we propose a new approach to improve the method of angular basis function (MABF) proposed by Young et al. (2015) for the Laplace equation in two-dimensional settings. Instead of the fundamental solution $\ln r$ used in the traditional Method of Fundamental Solution (MFS), MABF employs a different basis function θ and produces good approximate solutions on the domains with acute, narrow regions and exterior problems (Young et al., 2015). However, the definition of θ inevitably incurs a singularity situation for many different types of domains. Therefore, the selection of source points of MABF is not as convenient as the traditional MFS. To avoid the singularity situation in implementing, we introduce a transformation so that the transformed angular basis function does not exhibit this type of singularity for commonly used distributions of source points. As a result, source points for the method of transformed angular basis function (MTABF) can then be chosen in a similar way to traditional MFS. Numerical experiments demonstrate that the proposed approach significantly simplifies the selection of source points in MABF for different types of domains, which makes MABF more applicable. Numerical results of MTABF and MFS are presented for comparison purposes.

1. Introduction

The method of fundamental solution (MFS) was originally introduced by Kupradze and Aleksidze [11]. The implementation of MFS was studied for the first time by Mathon and Johnston [15]. MFS approximates the solution of the problem by a linear combination of fundamental solutions over a discrete set of source points placed outside of the domain. Therefore, the coefficients of the MFS approximation are determined by solving a linear problem. In the past two decades, MFS has attracted a lot of attentions from science and engineering community [2,5,8,10,12–14,16]. One of the main advantage of MFS is that it voids the complex mesh generations and numerical integrations. Survey papers of the MFS and related methods can be found in [4,6,7,9].

It is well-known that traditional method of fundamental solution (MFS) adopts the fundamental solution $\ln r$ of the 2-D Laplace equation. Actually, the function $\ln r$, as a function of the radial variable, is the real part of the complex fundamental solution of the Laplace equation. Through the complex variable theorem, the solution could be fully expressed in terms of radius and argument (see [3,17]). Furthermore, the imaginary part discussed in [3] can be simplified as a function of argument satisfying the Laplace equation when the source point is taken at the origin. This simplified function was called an angular basis function and has been used to construct the method of angular basis functions (MABF) in [17]. Therefore, MABF studied in [17] can be viewed as the MFS using this angular basis function, which is different from the traditional MFS using $\ln r$. MABF has been numerically shown to be a good substitute for the traditional method of fundamental solution (MFS) in solving the Laplace equation. However, to determine the locations of source points for this method is not straightforward. The authors of [17] proposed a distribution of source points to avoid any pair of a collocation point and a source points resting on a horizontal line so that the angular basis function $\theta(x, y)$ can be well defined. Therefore, there remains a crucial question of developing a simple approach for the selection of source points for MABF. Another study involving angular-type fundamental solution has been reported in [3] the Trefftz methods by using degenerate kernels and Fourier series to formulate the angular-type fundamental solution and then to successfully solve an infinite domain with circular holes and/or inclusions subject to a screw dislocation.

The aim of this paper is to develop an algorithm for MABF so that source points can be easily chosen as in MFS that uses radial basis function $\ln r$. Toward this end, we propose a transformation for angular basis function θ to avoid possible singular situations. The implementation of this transformation proceeds in three steps. Firstly, source points are

* Corresponding author.
E-mail addresses: xinxiang.lee@foxmail.com (X. Li), jaeyounroberts@gmail.com (J. Oh), wangyong@wustl.edu (Y. Wang), Huiqing.Zhu@usm.edu (H. Zhu).

https://doi.org/10.1016/j.enganabound.2018.04.001
Received 3 January 2018; Received in revised form 27 March 2018; Accepted 2 April 2018
Available online 24 April 2018

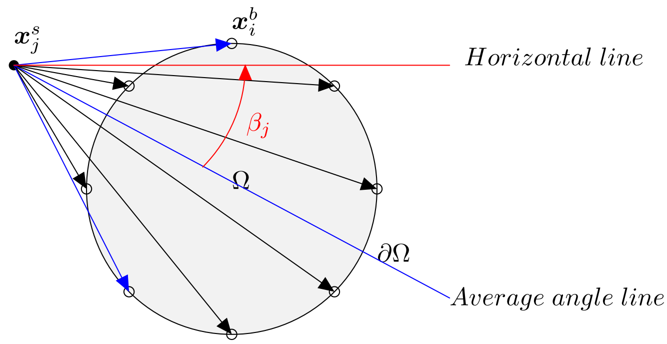

Fig. 1. The angle β_j for the transformation from Θ_{ij} to $\overline{\Theta}_{ij}$. Solid dot: a source point $\boldsymbol{x}_j^s$; open circles: boundary collocation points $\boldsymbol{x}_i^b$ for all $i = 1, 2, \ldots, N$.

placed surrounding the domain of the problem such that any source point should not stay interior of a convex region that contains all collocation points. Secondly, we calculate the average angle of all vectors pointing from a source point toward all collocation points. Then, we rotate all vectors about this source point through the average angle counterclockwise so that all angles are distributed quite evenly on $(-\pi/2, \pi/2)$. This process can be done by multiplying a rotation matrix generated by the average angle to each vector. As a result, all vectors are transformed to their reference positions (see Fig. 1). Thirdly, a transformed angular basis function (TABF) is then defined to be the direction angle of a transformed vector, which falls into $(-\pi/2, \pi/2)$. It can be verified that a TABF is also a fundamental solution of Laplace equation. The calculation of these TABFs on a set of source points results in the method of transformed angular basis function (MTABF), which can be seen as an improvement of MABF. Numerical experiments show that the effort in selecting source points is substantially reduced for different types of domains. Actually, many source point distributions that are commonly used in MFS also work for MTABF.

The rest of the paper is organized as follows: in Section 2 we introduce transformed angular basis functions. Formulation of MTABF is presented in Section 3. Numerical results and comparison are presented in Section 4. We end by some concluding remarks in Section 5.

2. Transformed angular basis functions

Let Ω be a bounded domain. Its boundary is denoted by $\partial\Omega$. Let

$$\boldsymbol{X}^b := \{\boldsymbol{x}_i^b = (x_i^b, y_i^b), i = 1 \ldots N\}$$

be a set of collocation points on $\partial\Omega$, and

$$\boldsymbol{X}^s := \{\boldsymbol{x}_j^s = (x_j^s, y_j^s), j = 1 \ldots N\}$$

be a set of source points on the boundary of a convex region containing Ω. Here, N denotes the number of collocation points. In this paper, we use the same number of source points as collocation points.

Furthermore, we denote by X and Y the distance matrices for variable x and y, respectively, i.e.,

$$X = \left(X_{ij}\right) \quad \text{and} \quad Y = \left(Y_{ij}\right), \tag{2.1}$$

where

$$X_{ij} := x_i^b - x_j^s, \quad \text{and} \quad Y_{ij} := y_i^b - y_j^s, \tag{2.2}$$

for any $i, j = 1 \ldots N$.

We now calculate the angle of each vector pointing from a source point $\boldsymbol{x}_j^s$ toward a boundary collocation point $\boldsymbol{x}_i^b$ with respect to x-axis. These angles can be written into the following original angular matrix

$$\Theta := \arctan\left(\frac{Y}{X}\right) = \begin{pmatrix} \Theta_{11} & \Theta_{12} & \ldots & \Theta_{1N} \\ \cdot & \cdot & \cdot & \cdot \\ \cdot & \cdot & \cdot & \cdot \\ \cdot & \cdot & \cdot & \cdot \\ \Theta_{N1} & \Theta_{N2} & \ldots & \Theta_{NN} \end{pmatrix} \tag{2.3}$$

Here each entry Θ_{ij} will be calculated by

$$\Theta_{ij} := \arctan\left(\frac{Y_{ij}}{X_{ij}}\right).$$

Note that function $\theta(x, y) := \arctan\frac{y}{x}$, that is known as the angular basis function (see [17]), can be used to construct the expression of the argument of complex number $z = x + iy$, which is usually denoted by $arg(z)$. A branch cut, usually along the negative real axis, can limit $arg(z)$ so it lies between $(-\pi, \pi]$. As pointed out in [17], the value of Θ_{ij} obtained from commonly used source point distributions would result in an ill-conditioning linear system. Therefore, the location of source points must be carefully determined. In order to alleviate the difficulty in choosing source points, we will design a transformation for Θ_{ij} so that source points can be selected in an easy way as for MFS. To illustrate this idea, we consider a disk domain Ω (see Fig. 1). We plot vectors $\overrightarrow{\boldsymbol{x}_j^s\boldsymbol{x}_i^b}$ $(i = 1, 2, \ldots, N)$ from a given source point $\boldsymbol{x}_j^s$ toward all collocation points $\boldsymbol{x}_i^b$ on the boundary $\partial\Omega$.

We first find the average angle line by averaging the maximal and minimal angles among all angles of these vectors. Then an angle $\beta \in [0, 2\pi)$ between the average angle line and the horizonal line can be figured out. Secondly, we transform all vectors by using a rotation matrix with angle β_j so that angles of these transformed vectors fall into the interval $(-\pi/2, \pi/2)$. This transformation can be designed for any given domain if the locations of sources points are properly selected.

2.1. Calculation of β

Next, we will give a detailed description about the calculation of angle β_j that labeled in Fig. 1. Without loss of generality, we work out β_j for vectors $\overrightarrow{\boldsymbol{x}_j^s\boldsymbol{x}_i^b}$ $(i = 1, 2, \ldots, N)$. The β values for vectors starting from other source points can be found in a similar manner. Actually, we have

$$\beta_j = \begin{cases} \pi - \frac{1}{2}(\gamma_1 + \gamma_2), & \text{if} \quad \gamma_3 - \gamma_4 > \pi \text{ and } \gamma_3 + \gamma_4 \le 2\pi, \\ 3\pi - \frac{1}{2}(\gamma_1 + \gamma_2), & \text{if} \quad \gamma_3 - \gamma_4 > \pi \text{ and } \gamma_3 + \gamma_4 > 2\pi, \\ 2\pi - \frac{1}{2}(\gamma_3 + \gamma_4), & \text{otherwise,} \end{cases} \tag{2.4}$$

where

$$\begin{aligned} \gamma_1 &:= \max\{\vartheta \in \{\theta_{ij}\}_{i=1}^N \mid \vartheta < \pi\}, & \gamma_2 &:= \min\{\vartheta \in \{\theta_{ij}\}_{i=1}^N \mid \vartheta > \pi\}, \\ \gamma_3 &:= \max\{\theta_{ij}\}_{i=1}^N, & \gamma_4 &:= \min\{\theta_{ij}\}_{i=1}^N, \\ \theta_{ij} &:= arg(z_{ij}), & z_{ij} &:= (x_i^b - x_j^s) + \boldsymbol{i}(y_i^b - y_j^s). \end{aligned}$$

Multiplying the rotation matrix on each vector $\overrightarrow{\boldsymbol{x}_j^s\boldsymbol{x}_i^b}$ we obtain

$$\begin{bmatrix} \overline{X}_{ij} \\ \overline{Y}_{ij} \end{bmatrix} = \begin{pmatrix} \cos\beta & -\sin\beta \\ \sin\beta & \cos\beta \end{pmatrix} \begin{bmatrix} X_{ij} \\ Y_{ij} \end{bmatrix}. \tag{2.5}$$

As a consequence, each entry of matrix Θ can be transformed into a new matrix $\overline{\Theta}$ as follows

$$\overline{\Theta} := \arctan\left(\frac{\overline{Y}}{\overline{X}}\right) = \left(\arctan\left(\frac{\overline{Y}_{ij}}{\overline{X}_{ij}}\right)\right)_{N\times N}. \tag{2.6}$$

We already complete the design of the transformation for the angle matrix Θ. Next, we will consider the transformation of the angular basis function.

2.2. The ABF $\phi(x, y) = \theta$ and the corresponding TABF $\varphi(x, y) = \overline{\theta}$

Consider the angular basis function (see [17]):

$$\phi(x, y) = \theta = \arctan\left(\frac{Y}{X}\right),$$

where $\langle X, Y\rangle = \langle x - x_0, y - y_0\rangle$ denotes a vector in xy-plane starting at (x_0, y_0). It is straightforward to verify that $\theta(x, y)$ is a fundamental solution of the Laplace equation. We define the transformed angular basis

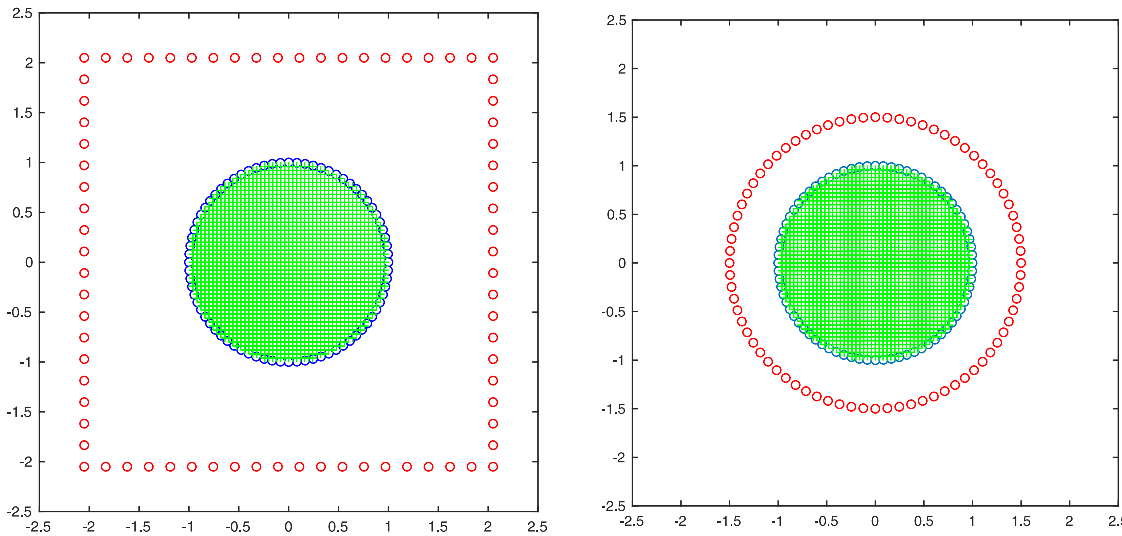

Fig. 2. Left Plot: Boundary collocation points (Blue) and source points distributed on a square (Red); Right Plot: boundary collocation points (Blue) and source points distributed on a circle (Red). (For interpretation of the references to color in this figure legend, the reader is referred to the web version of this article).

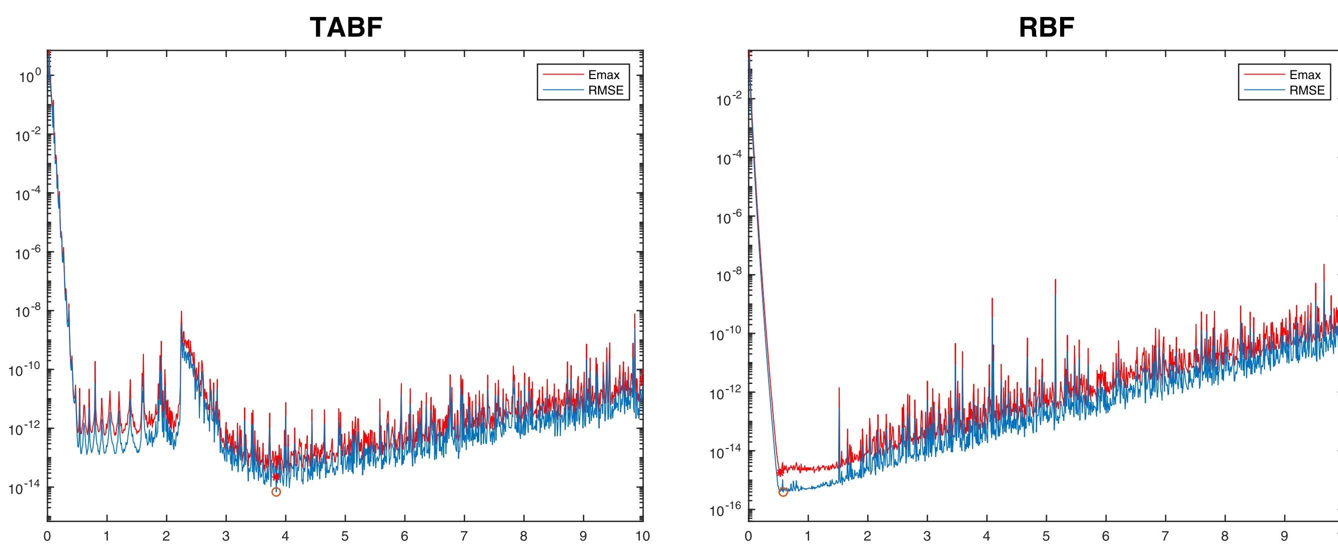

Fig. 3. Error curves of MFS using TABF (Left Plot) and RBF (Right Plot) w.r.t. distance d when $N = 80$ source points are used.

Table 1
Errors of MTABF.

N	RMSE	e_{max}	d_1	d_2	Cond.
30	7.3565E−13	1.1047E−11	6.04	2.18	1.4507E+16
40	2.8204E−14	1.1635E−13	1.92	1.92	1.1897E+18
50	1.7240E−14	4.8406E−14	5.21	5.21	2.7277E+18
60	9.6974E−15	3.5083E−14	3.69	4.59	3.7423E+18
70	6.6166E−15	1.9540E−14	3.64	3.64	2.5692E+19
80	6.8347E−15	2.2204E−14	3.84	3.84	4.2459E+18
90	7.9716E−15	2.7423E−14	3.56	3.65	1.3031E+19
100	9.3305E−15	2.5979E−14	3.44	3.64	6.3588E+18

function $\varphi(x, y)$ as follows:

$$\varphi(x, y) := \bar{\theta} = \arctan\left(\frac{\overline{Y}}{\overline{X}}\right), \tag{2.7}$$

where

$$\begin{bmatrix}\overline{X}\\ \overline{Y}\end{bmatrix} = \begin{pmatrix}\cos\beta & -\sin\beta\\ \sin\beta & \cos\beta\end{pmatrix}\begin{bmatrix}X\\ Y\end{bmatrix}$$

for a given $\beta \in [0, 2\pi)$.

Theorem 2.1. *Assume that $(x_0, y_0) \notin \overline{\Omega}$. Then the function $\varphi(x, y)$ defined in (2.7) is a fundamental solution of the Laplace equation, i.e.,*

$$\Delta\varphi(x, y) = 0, \quad \text{on } \Omega. \tag{2.8}$$

Proof. Note that $\varphi(x, y) = \bar{\theta}$. By direct calculation, one has

$$\begin{aligned}\frac{\partial^2\bar{\theta}}{\partial x^2} &= \frac{\partial}{\partial x}\left[\frac{\sin\beta\overline{X} - \cos\beta\overline{Y}}{\overline{X}^2 + \overline{Y}^2}\right]\\ &= -\frac{2}{\left(\overline{X}^2 + \overline{Y}^2\right)^2}\left[\overline{X}\,\overline{Y}\left(\sin^2\beta - \cos^2\beta\right) + \left(\overline{X}^2 - \overline{Y}^2\right)\sin\beta\cos\beta\right].\end{aligned} \tag{2.9}$$

Meanwhile, we have

$$\begin{aligned}\frac{\partial^2\bar{\theta}}{\partial y^2} &= \frac{\partial}{\partial y}\left[\frac{\cos\beta\overline{X} + \sin\beta\overline{Y}}{\overline{X}^2 + \overline{Y}^2}\right]\\ &= \frac{2}{\left(\overline{X}^2 + \overline{Y}^2\right)^2}\left[\overline{X}\,\overline{Y}\left(\sin^2\beta - \cos^2\beta\right) + \left(\overline{X}^2 - \overline{Y}^2\right)\sin\beta\cos\beta\right].\end{aligned} \tag{2.10}$$

Table 2
Errors of MFS using RBF.

N	RMSE	e_{max}	d_1	d_2	Cond.
30	2.0568E−113	1.4655E−12	6.38	5.21	1.6760E+17
40	6.6359E−16	6.6613E−15	1.86	1.61	8.3350E+17
50	4.1191E−16	1.7764E−15	1.1	1.12	6.1203E+18
60	3.7088E−16	2.2204E−15	0.98	0.86	1.7987E+18
70	3.8737E−16	2.2204E−15	0.66	0.77	2.7732E+18
80	3.9322E−16	1.7764E−15	0.53	0.58	3.0972E+18
90	4.0149E−16	2.2204E−15	0.46	0.5	1.2992E+19
100	4.2694E−16	2.2204E−15	0.83	0.65	3.1384E+18

Therefore, by adding (2.9) and (2.10) we obtain

$\Delta\varphi(x, y) = \Delta\bar{\theta} = 0.$

□

Remark 2.2. It is clear that by setting $(x_0, y_0) = \boldsymbol{x}_j^s$, we get a group of transformed angular basis functions $\varphi_j(x, y)$, $j = 1, 2, \ldots, N$ satisfying

$$\varphi_j(\boldsymbol{x}_i^b) = \overline{\Theta}_{ij}. \tag{2.11}$$

Furthermore, function $\bar{\theta} + C$ also defines a transformed angular basis function for any fixed constant C.

3. Formulation of MTABF

We consider the Laplace equation with boundary conditions:

$$\begin{aligned} \Delta u &= 0 \quad \text{in } \Omega, \\ u &= g_1 \quad \text{on } \partial\Omega_1, \\ \frac{\partial u}{\partial n} &= g_2 \quad \text{on } \partial\Omega_2, \end{aligned} \tag{3.1}$$

where $\partial\Omega$ is the boundary of Ω, and $\partial\Omega = \partial\Omega_1 \cup \partial\Omega_2$.

We assume that MTABF approximation to the solution of Problem (3.1) can be written as follows:

$$\widetilde{u} := \sum_{j=1}^{N} \alpha_j \varphi_j(x, y). \tag{3.2}$$

where φ is defined in (2.7). It is straightforward to verify that the MTABF approximation $\widetilde{u}$ satisfies the Laplace equation. By (2.11), the numerical solutions can be solved from the following linear system

$$\overline{\Theta}\,\boldsymbol{\alpha} = \boldsymbol{g} \tag{3.3}$$

where $\boldsymbol{\alpha} = (\alpha_1, \alpha_2, \ldots, \alpha_N)^T$, and $\boldsymbol{g} = \left(g(\boldsymbol{x}_1^b), g(\boldsymbol{x}_2^b), \ldots, g(\boldsymbol{x}_N^b)\right)^T$.

4. Numerical experiments

In this section, we consider Problem (3.1) on several simply connected domains in $\mathbb{R}^2$. Suppose that $u(x, y)$ and $\tilde{u}(x, y)$ are the exact solution and its MTABF approximation, respectively. The error between u and $\tilde{u}$ will be measured by $E_{\max}$ and RMSE, which are defined as follows:

$$\begin{aligned} E_{\max} &= \max_{k=1,\ldots,M} \left| u(\boldsymbol{x}_k^t) - \tilde{u}(\boldsymbol{x}_k^t) \right|, \\ \text{RMSE} &= \sqrt{\frac{1}{M}\sum_{k=1}^{M} \left(u(\boldsymbol{x}_k^t) - \tilde{u}(\boldsymbol{x}_k^t)\right)^2}. \end{aligned} \tag{4.1}$$

where test points $\left\{\boldsymbol{x}_k^t,\ \ k = 1, 2, \ldots, M\right\}$ are uniformly distributed in Ω.

The numerical results show that MTABF produces accurate numerical approximation which is comparable to traditional MFS which uses a RBF $\ln r$, i.e., the fundamental solution of 2d Laplace equation. In particular, in Examples 4.3 and4.4, we consider the same numerical examples as those studied in [17], so that the improvement of the algorithm by using TABF can be clearly observed from the distribution of the source points. These examples verify that MTABF does not require any special source point distribution in the computation. All numerical examples provided in this section adopt similar source point distributions as that of traditional MFS.

Example 4.1. In this example, we consider Problem (3.1) on a disk domain with a harmonic boundary condition $g_1 = e^x \cos y$ on $\partial\Omega$.

The purpose of this example is to validate the efficiency of the proposed algorithm. It can be seen later from numerical results that MTABF is comparable with the traditional MFS.

We consider two types of source points that are distributed on a square and a circle (see Fig. 2). There are 76 source points and boundary collocation points in both graphs. For simplicity, we only use uniformly distributed source points and boundary collocation points.

Let d be the distance between the circle of source points and the boundary of Ω. Different d values are used to test the accuracy of the MFS approximation using the transformed angular basis function $\overline{\theta}$. It has been known that if angular basis function θ is used instead, a specially designed distribution of source points is required to obtain decent results (see [17, Figure 5]).

Next, we present numerical results of the proposed method when source points are distributed on a circle and a square.

(1) *Source points distributed on a circle outside of* $\partial\Omega$. To increase the stability, source points are slightly rotated counterclockwise by an an-

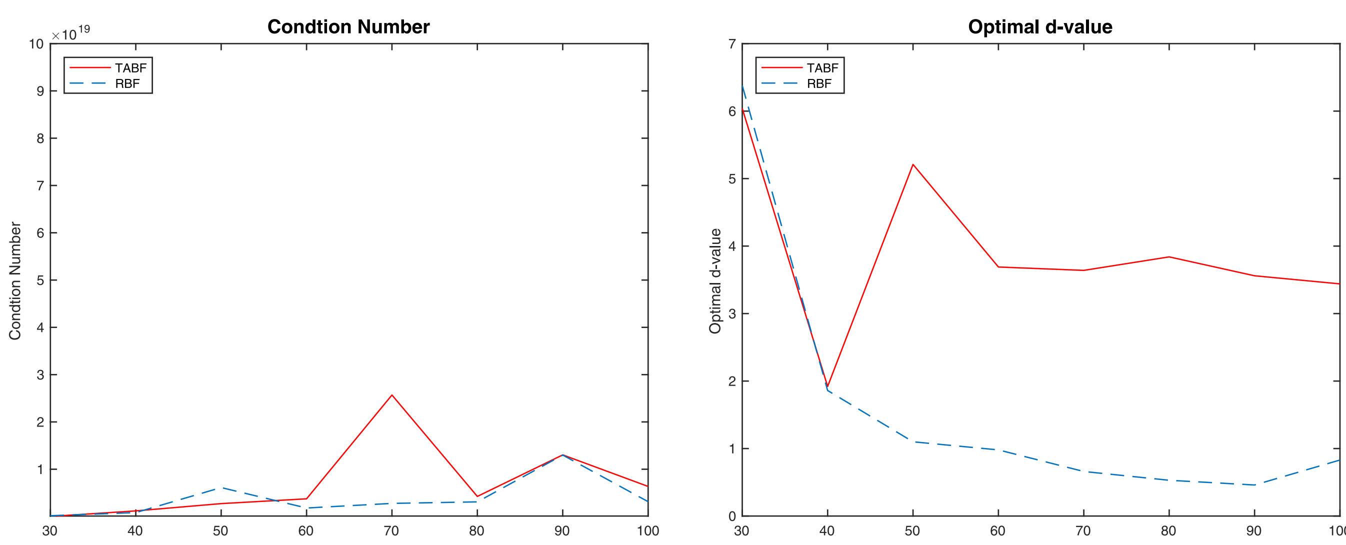

Fig. 4. Condition numbers of coefficient matrices in MFS using TABF (Left Plot) and RBF (Right Plot) w.r.t. N.

Table 3
Errors of MFS using TABF.

N	RMSE	e_{max}	d_1	d_2	Cond.
28	3.4880E−12	1.5430E−11	9.92	9.99	1.8255E+17
40	5.8142E−14	2.1894E−13	4.88	5.06	7.4657E+17
48	2.8842E−14	7.8049E−14	3.4	3.4	7.9216E+17
60	9.9171E−16	3.9968E−15	1.66	1.82	4.6207E+18
68	6.2346E−16	3.1086E−15	1.63	1.47	4.1120E+18
80	7.3680E−16	4.6629E−15	1.3	1.42	3.8081E+18
88	7.0708E−16	3.9968E−15	1.48	1.38	3.0443E+19
100	9.7743E−16	3.4417E−15	1.25	1.25	4.8391E+18

Table 4
Errors of MFS using RBF.

N	RMSE	e_{max}	d_1	d_2	Cond.
28	5.8499E−11	2.4394E−10	8.02	8.02	3.5970E+17
40	2.7687E−14	2.1605E−13	2.84	2.66	3.8882E+18
48	5.5865E−15	2.1316E−14	2.86	2.99	1.0617E+18
60	1.5924E−15	6.5503E−15	1.85	1.78	9.0967E+17
68	1.1259E−15	4.2188E−15	1.43	1.43	3.1119E+18
80	7.1544E−16	2.4980E−15	1.01	1.01	3.1133E+18
88	6.6540E−16	2.6645E−15	0.95	0.97	6.8904E+18
100	6.0403E−16	2.6645E−15	0.85	0.82	8.1619E+18

gle $\epsilon = \frac{2}{\pi}$. The values of distance where minimal E_{max} and RMSE are observed are denoted by d_1 and d_2, respectively. Table 1 demonstrates the efficiency of the proposed method by showing the E_{max} and RMSE with respect to different number of source and collect points, while $M = 1941$ testing points are used in the calculation of E_{max} and RMSE. The condition number of the coefficient matrix, d_1, d_2 are also listed. Additionally, we present numerical approximation by using MFS with RBF $\ln r$ in Table 2. It can be seen that both methods can solve this problem efficiently and produce comparable numerical approximations. To compare these two methods from other points of view, we plot the error curves of these two methods with respect to the distance d in Fig. 3, and condition numbers of coefficient matrices in these two methods with respect to the number of collocation points N in Fig. 4.

(2) *Source points distributed on a square outside of* $\partial\Omega$. For the same reason as in (1), we rotate all source points counterclockwise by $h = 0.1$ along the square. Similar numerical results as in (1) are presented here in Tables 3, 4, and Fig. 5.

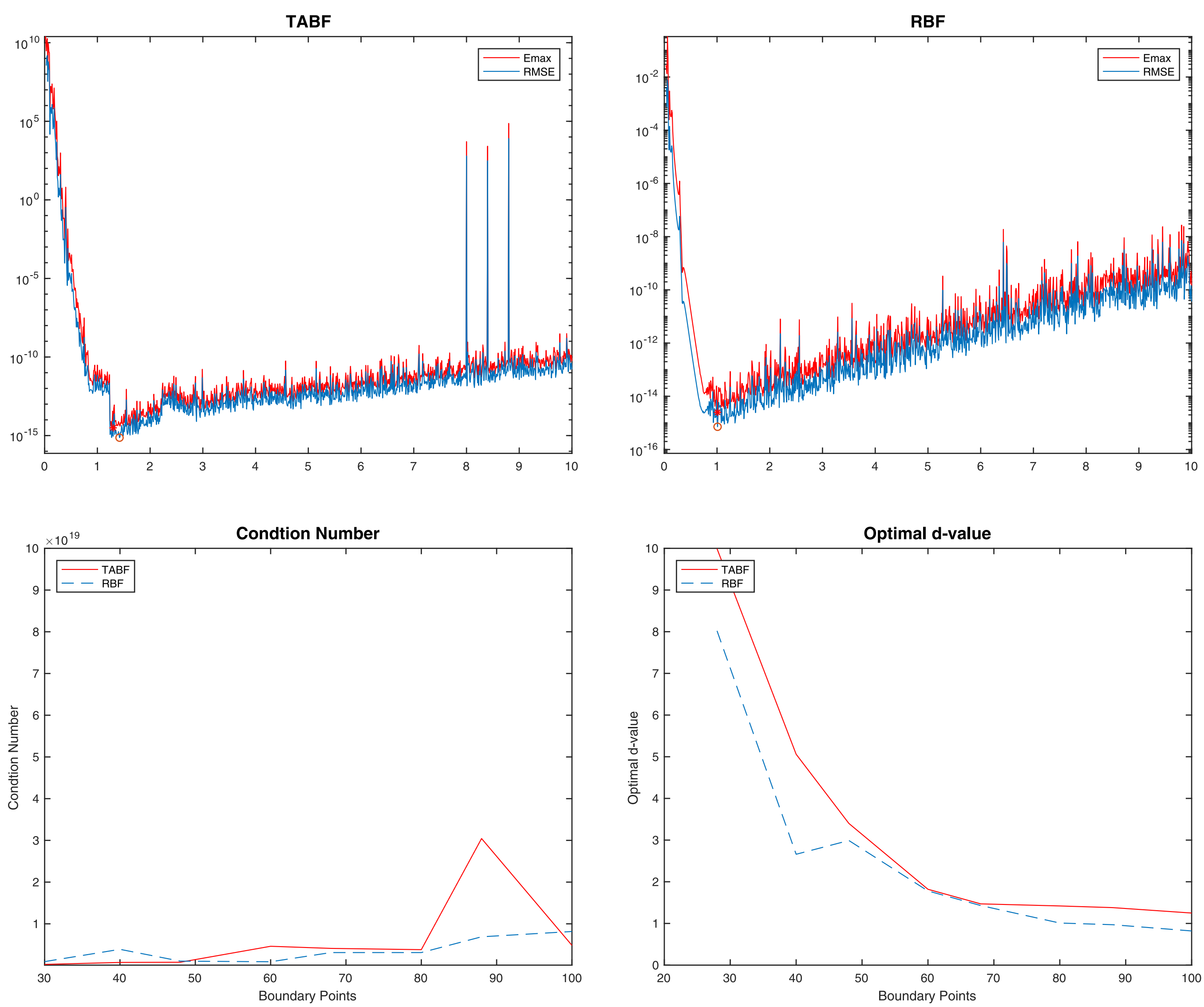

Fig. 5. Upper Plots: error curves of MFS using TABF (Left Plot) and RBF (Right Plot) w.r.t. distance d when $N = 80$ source points are used. Lower Plots: condition numbers of coefficient matrices in MFS using TABF (Left Plot) and RBF (Right Plot) w.r.t. N.

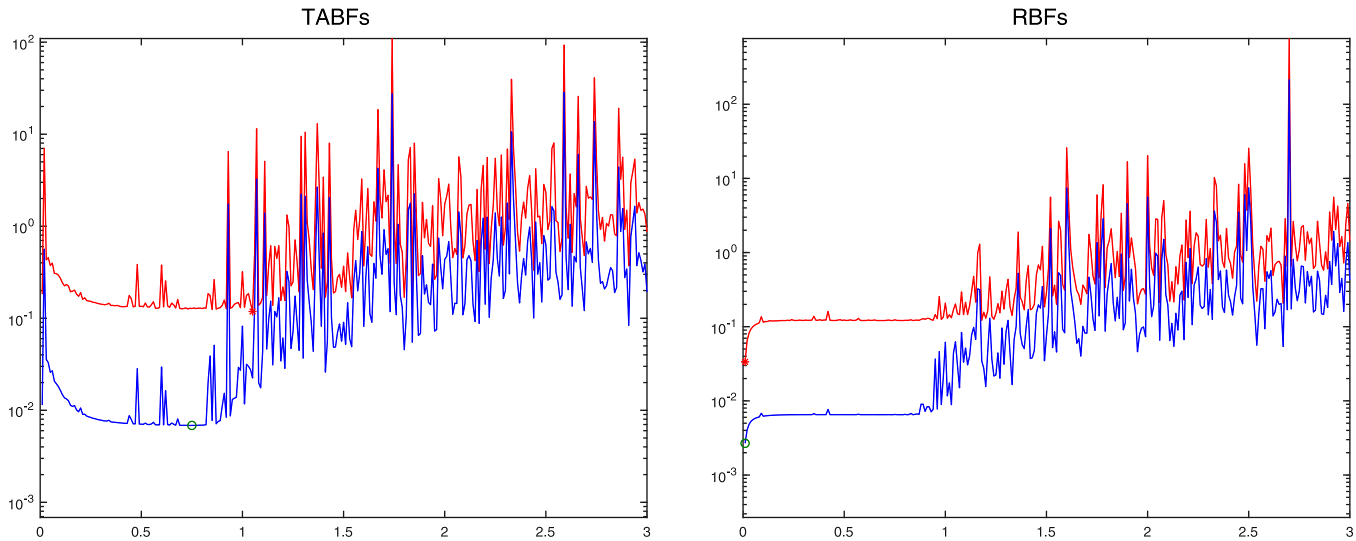

Fig. 6. Maximum errors (Red) and RMSE errors (Blue) when source points on a square are used. Left Plot: MFS using TABF $\overline{\theta}$; Right Plot: MFS using RBF $\ln r$. (For interpretation of the references to color in this figure legend, the reader is referred to the web version of this article).

Table 5
Minimum values of maximum errors and RMSE errors in Fig. 4.

	Source points on a square		Source points on a circle	
Method	RMSE	e_{max}	RMSE	e_{max}
TABF	6.800e−03	1.274e−01	2.000e−03	3.380e−02
RBF	2.700e−03	3.360e−02	6.500e−03	1.213e−01

Example 4.2. As an extension of Example 4.1, we consider a non-smooth boundary condition:

$$
\begin{aligned}
&u = 0, \quad \theta = 0, \theta = \pi,\\
&u = 1, \quad 0 \le \theta \le \pi, \qquad (4.2)\\
&u = -1, \quad \pi \le \theta \le 2\pi,
\end{aligned}
$$

so that analytical solution can be found as follows:

$$u = \frac{2}{\pi} \arctan\left(\frac{2y}{1 - x^2 - y^2}\right). \qquad (4.3)$$

We also consider source points on a circle and a square. Due to the discontinuity of the boundary condition, the approximation error in a neighbourhood of the discontinuity points becomes very large so that it pollutes the global errors E_{max} and RMSE. For source points distributed on a circle, we plot error curves of MFS using TABF and RBF in Fig. 6 with the same value of M as in Example 4.1. Minimum values of these error curves are reported in Table 5.

Similarly, rotating source points slightly by an angle ϵ along the circle as we did in Example 4.1 improves the stability of the proposed method. However, the value of ϵ does not significantly affect the error if ϵ are properly chosen so that source points and collocation points do not stay on a radian line. Table 6 presents E_{max} and RMSE and corresponding d-values when several different values of ϵ are used. The error curves of MFS using TABF are plotted in Fig. 7 (Left) when $\epsilon = 0.01$. It can be seen that both error curves of the MFS using TABF do not exhibit oscillation when $d < 1.3$. Meanwhile, the right plot in Fig. 7 shows the errors of MFS using the RBF $\ln r$, which is quite stable when $d < 1.5$. Minimum values of E_{max} and RMSE are listed in Table 5.

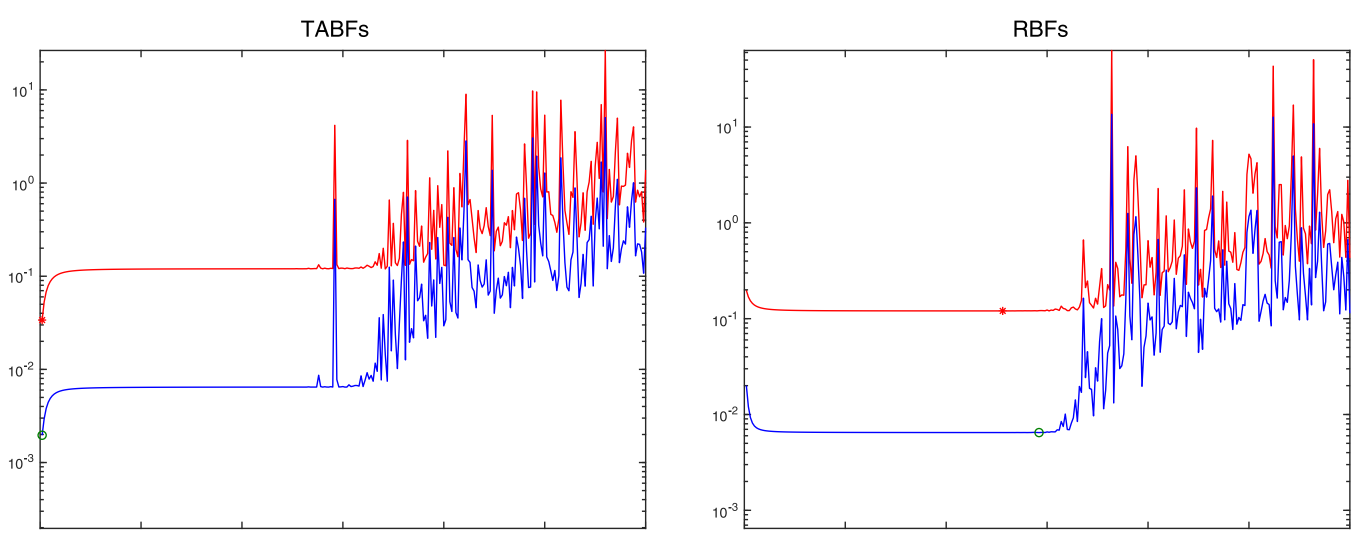

Fig. 7. Maximum errors (Red) and RMSE errors (Blue) when shifted source points on a circle (with $\epsilon = 0.01$) are used. Left Plot: MFS using TABF $\overline{\theta}$; Right Plot: MFS using RBF $\ln r$. (For interpretation of the references to color in this figure legend, the reader is referred to the web version of this article).

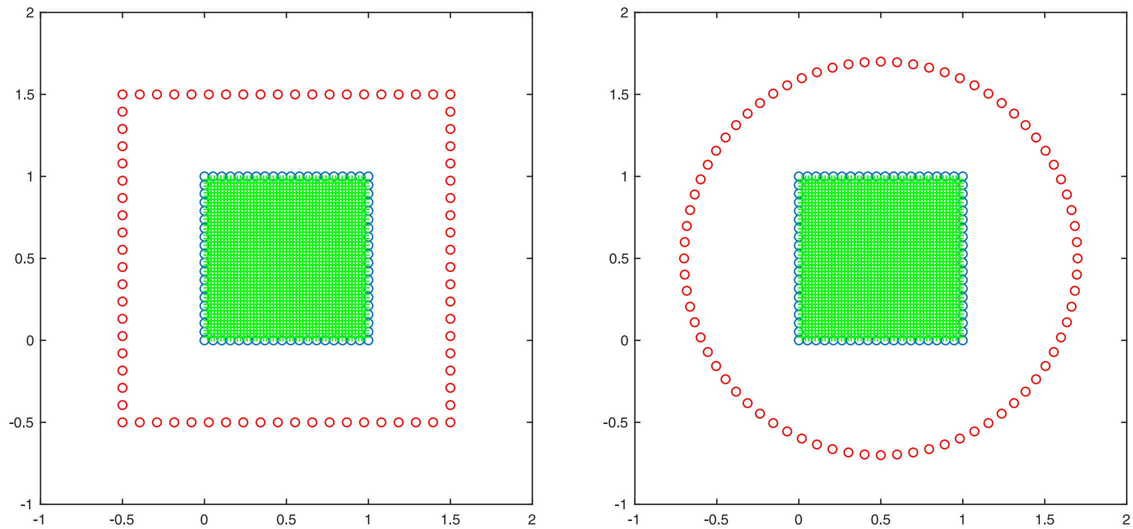

Fig. 8. Boundary collocation points (Blue); source points on a square (Red, Left Plot); source points on a circle (Red, Right Plot); $N = 50$. (For interpretation of the references to color in this figure legend, the reader is referred to the web version of this article).

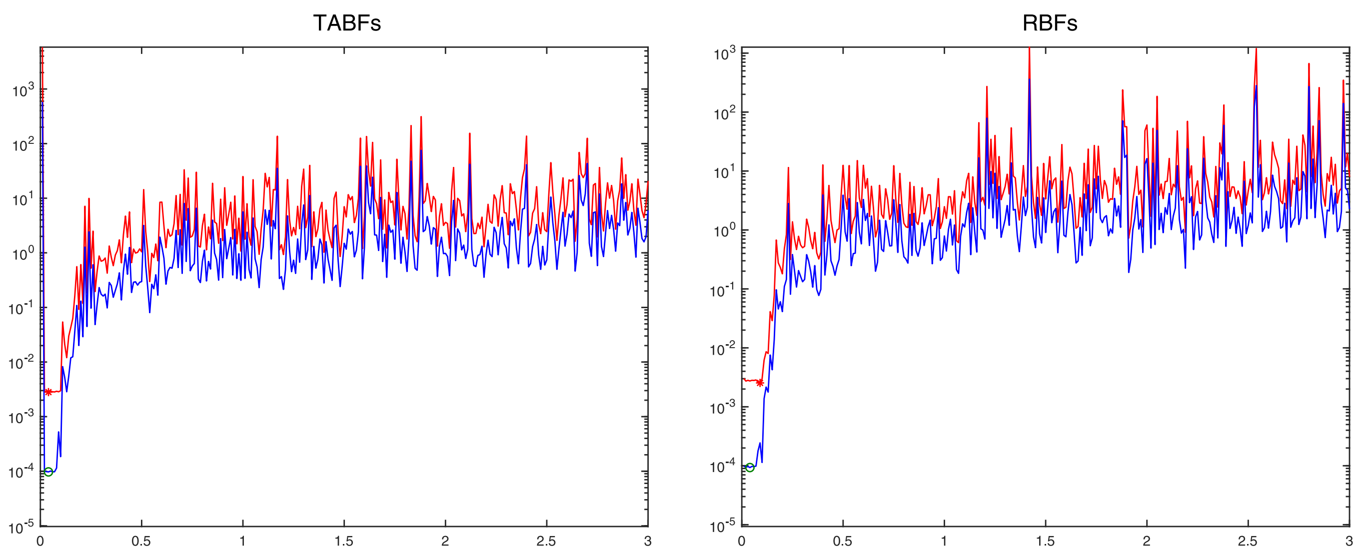

Fig. 9. Maximum errors (Red) and RMSE errors (Blue) when source points are distributed on a square. Left Plot: MTABF; Right Plot: MFS using $\ln r$. (For interpretation of the references to color in this figure legend, the reader is referred to the web version of this article).

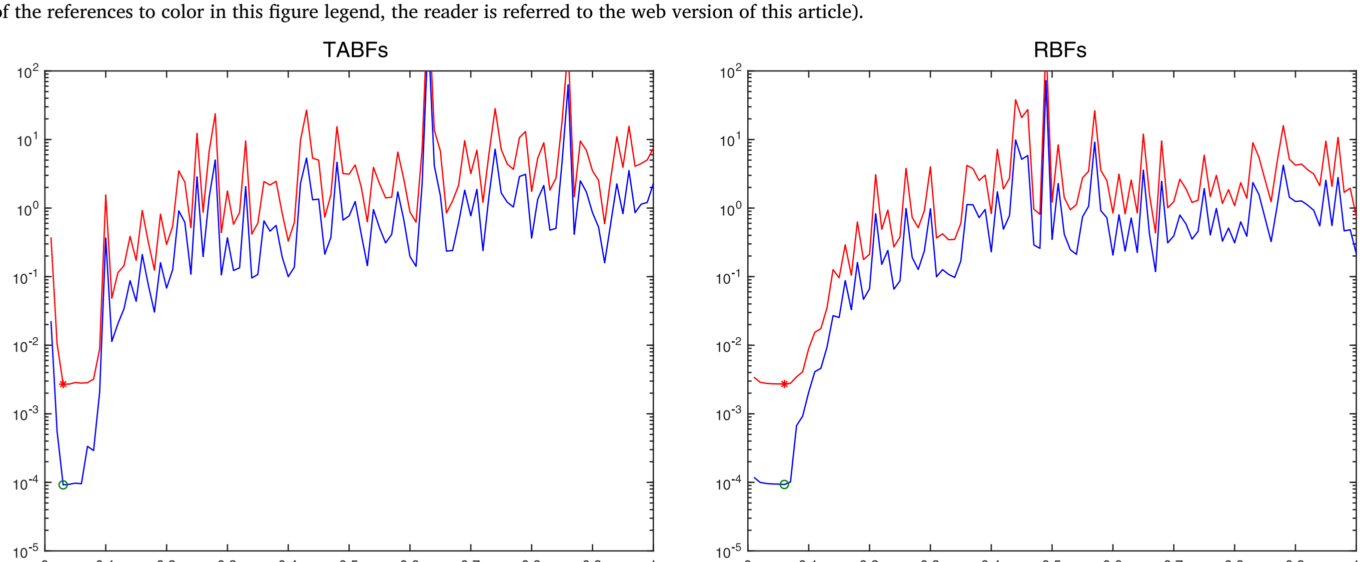

Fig. 10. Maximum errors (Red) and RMSE errors (Blue) when source points are distribute on a circle. Left Plot: MTABF; Right Plot: MFS using $\ln r$. (For interpretation of the references to color in this figure legend, the reader is referred to the web version of this article).

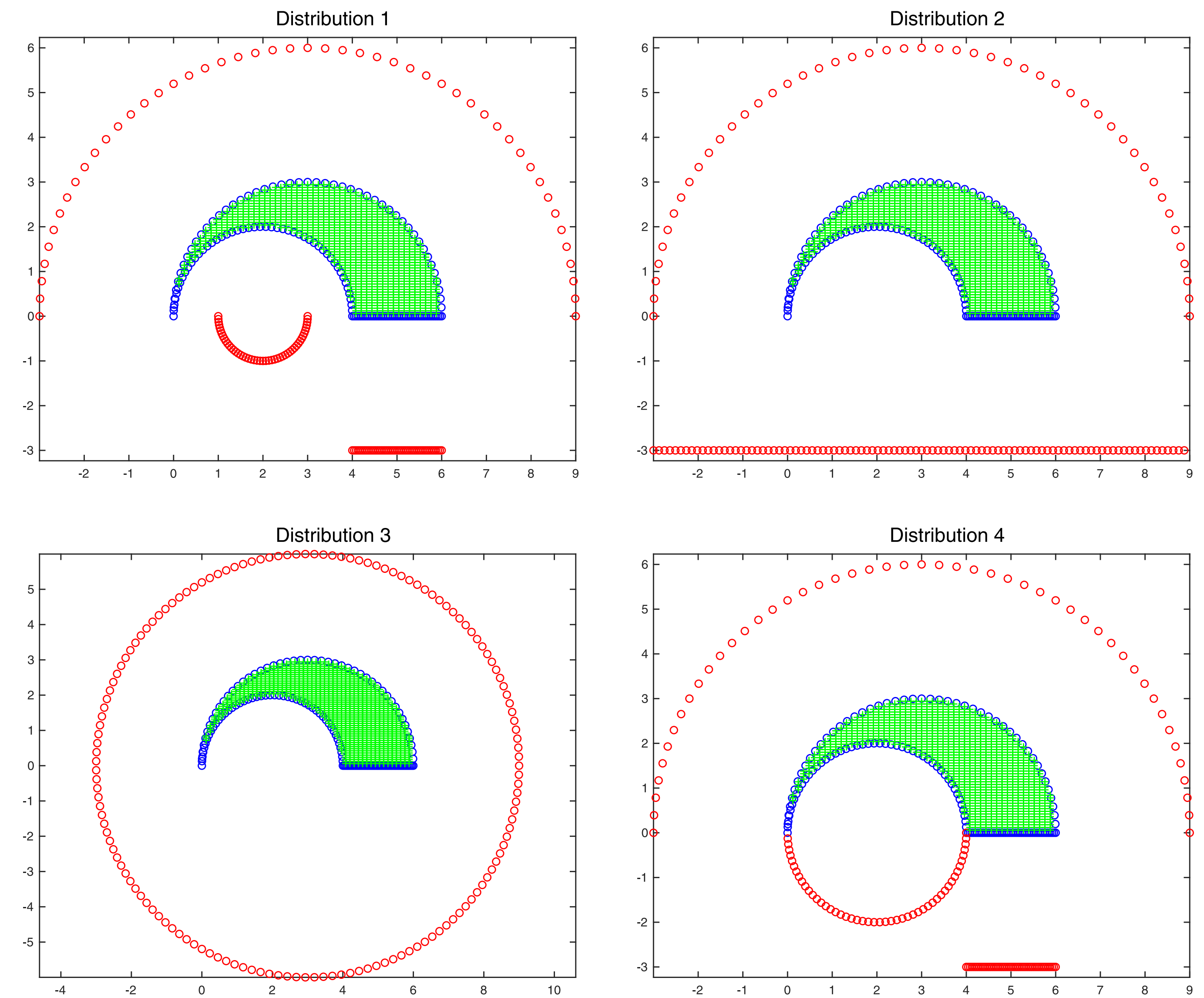

Fig. 11. Four different distributions of source points (Red) and boundary collocation points (Blue). $N = 147$. (For interpretation of the references to color in this figure legend, the reader is referred to the web version of this article).

Table 6
Minimum values of maximum errors and RMSE errors when source points are shifted ϵ units counterclockwise.

ϵ	r	RMSE	e_{max}
0.01	1.001	5.700e−03	6.490e−02
	1.005	2.100e−03	2.620e−02
	1.01	2.000e−03	3.380e−02
	1.05	4.900e−03	8.750e−02
	1.1	5.900e−03	1.070e−01
0.1	1.001	2.380e−02	3.430e−01
	1.005	7.700e−03	1.234e−01
	1.01	5.100e−03	8.190e−02
	1.05	5.100e−03	9.230e−02
	1.1	5.900e−03	1.082e−01
0.2	1.001	2.950e−02	4.092e−01
	1.005	1.220e−02	2.017e−01
	1.01	7.100e−03	1.267e−01
	1.05	5.400e−03	9.820e−02
	1.1	6.000e−03	1.100e−01
0.3	1.001	3.100e−02	4.267e−01
	1.005	1.560e−02	2.546e−01
	1.01	8.900e−03	1.640e−01
	1.05	5.600e−03	1.035e−01
	1.1	6.100e−03	1.118e−01

Table 7
Minimum values of e_{max} and RMSE in Figs. 9 and 10.

	Source points on a square		Source points on a circle	
Method	RMSE	e_{max}	RMSE	e_{max}
TABFs	9.7175e−05	2.800e−03	9.1818e−05	2.700e−03
RBFs	9.3104e−05	2.500e−03	9.3063e−05	2.700e−03

Example 4.3. We consider an example studied in [17, Section 4.1.1], which is the Laplace equation defined on a square domain $[0, 1] \times [0, 1]$ with a non-smooth boundary condition:

$$\begin{aligned} u &= 0, \quad \text{if} \quad x = 0, \\ u &= 0, \quad \text{if} \quad x = 1, \\ u &= 0, \quad \text{if} \quad x = y = 0, \\ u &= 1, \quad \text{if} \quad x = y = 1. \end{aligned} \tag{4.4}$$

The analytical solution is therefore given by

$$u = \sum_{j=1}^{\infty} \frac{2(1 - \cos(j\pi))\sinh(j\pi y)\sin(j\pi x)}{j\pi \sinh(j\pi)}. \tag{4.5}$$

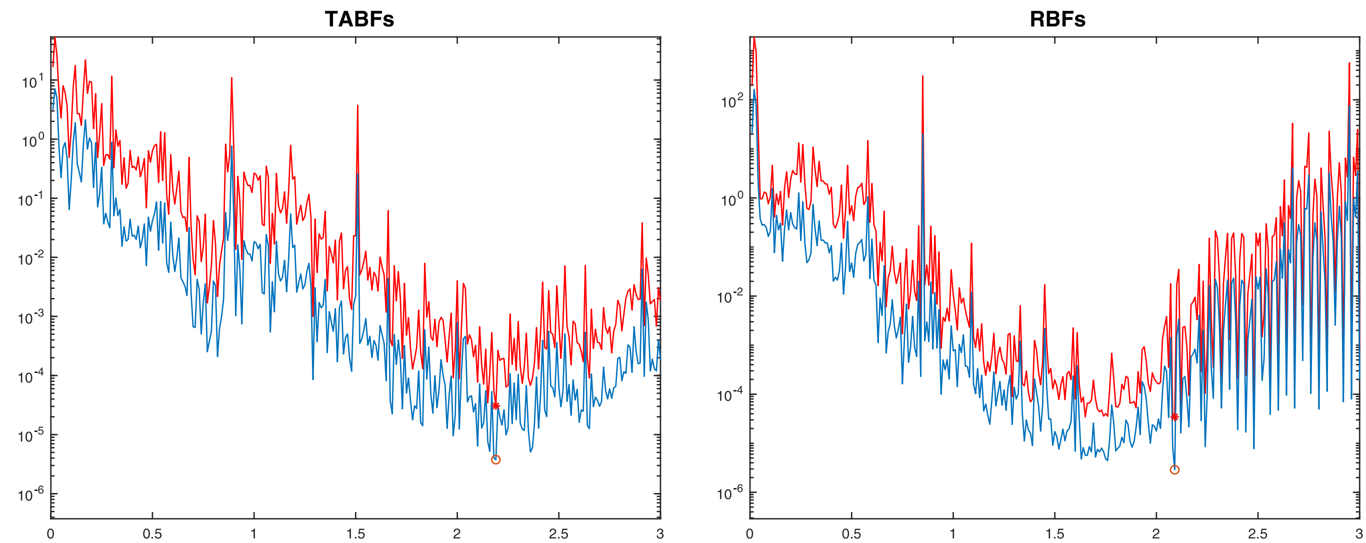

Fig. 12. Maximum error (Red) and RMSE (Blue) when distribution 1 is used. (For interpretation of the references to color in this figure legend, the reader is referred to the web version of this article).

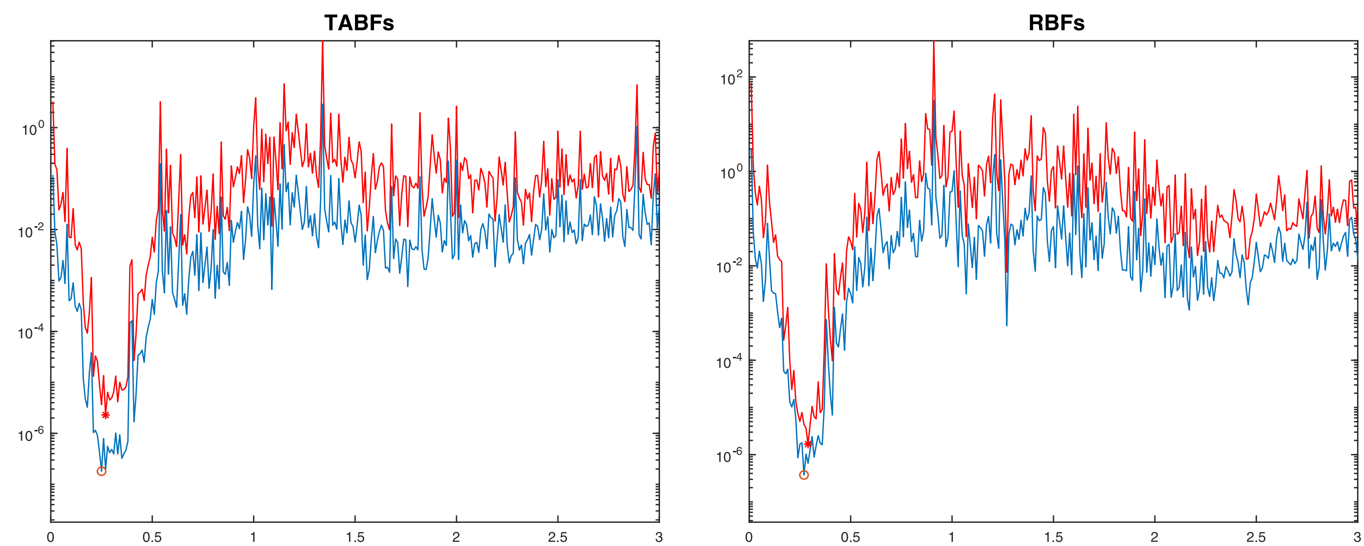

Fig. 13. Maximum error (Red) and RMSE (Blue) when distribution 2 is used. (For interpretation of the references to color in this figure legend, the reader is referred to the web version of this article).

Table 8
Minimum values of RMSE and Maximum error when distribution 4 is used.

Method	RMSE	e_{max}	RMSE	e_{max}
	Distribution 1		Distribution 2	
TABFs	$1.0406e{-}04$	$4.5183e{-}04$	$1.8407e{-}07$	$3.9079e{-}06$
RBFs	$4.4530e{-}05$	$2.7909e{-}04$	$8.4695e{-}07$	$2.4744e{-}06$
	Distribution 3		Distribution 4	
TABFs	$1.5200e{-}02$	$1.5430e{-}01$	$9.9381e{-}05$	$4.1424e{-}04$
RBFs	$1.6200e{-}02$	$1.2100e{-}01$	$7.6895e{-}05$	$3.8910e{-}04$

In [17], a comparison of MFS approximation contour and MABF approximation contour showed that both methods generated decent results. However, MABF did not generate a good approximation if source points were evenly distributed outside the domain. Therefore, the location of source points in MABF needs to be specially designed to avoid the singularity of the angular basis function. In this example, we compare MTABF approximation with MFS approximation defined on similar distributions of source points. More specifically, we use the two types of source points defined in Examples 4.1 and 4.2 (see Fig. 8). For both cases, N source points are equally distributed. We use $M = 2400$ testing points for the calculation of the error. Similar numerical results are observed as in Example 4.2. Fig. 9 and Fig. 10 plot the error curves of MFS and MABF, respectively, with respect to the distance d. The minimum errors of both methods are listed in Table 7.

Example 4.4. In this example, we consider a domain with a cusp-point (see Fig. 11). There are many engineering applications where cusp problems are encountered [1,8,16].

We choose the following boundary condition

$$\begin{aligned} &u = 0, && \text{if} \quad r = 2, \quad 0 \le \theta \le \pi, \\ &\frac{\partial u}{\partial n} = 0, && \text{if} \quad 2 \le r \le 3, \quad \theta = 0, \\ &u = 1, && \text{if} \quad r = 3, \quad 0 \le \theta \le \pi. \end{aligned} \tag{4.6}$$

The analytical solution is given by (see [17])

$$u = 3 - \frac{12x}{x^2 + y^2}. \tag{4.7}$$

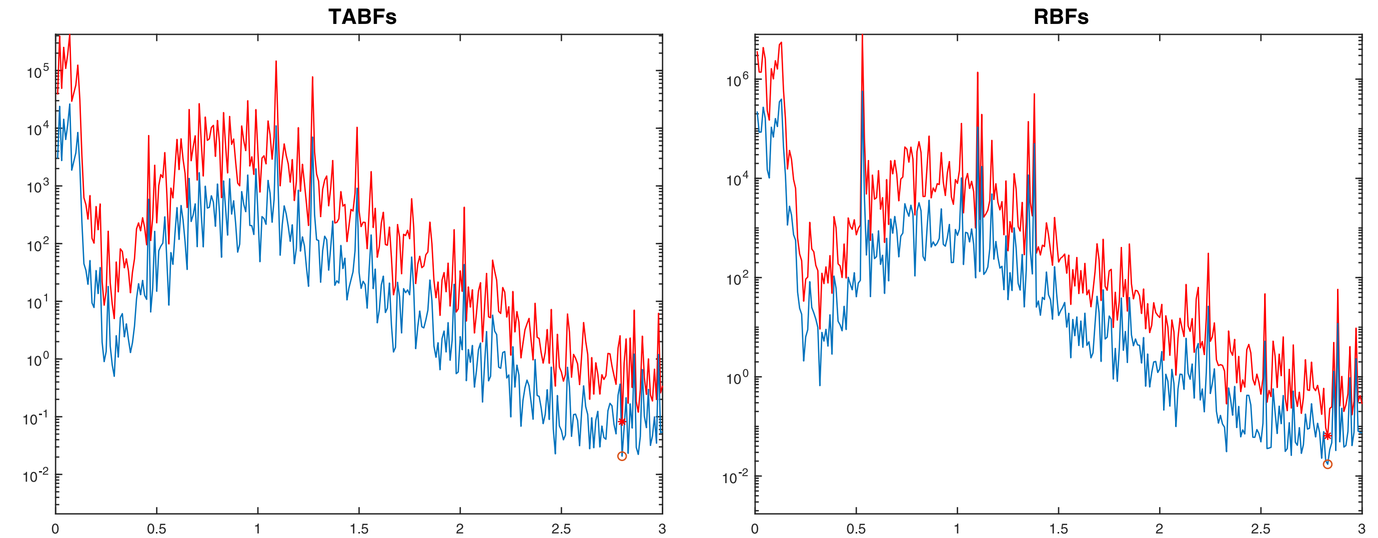

Fig. 14. Maximum error (Red) and RMSE (Blue) when distribution 3 is used. (For interpretation of the references to color in this figure legend, the reader is referred to the web version of this article).

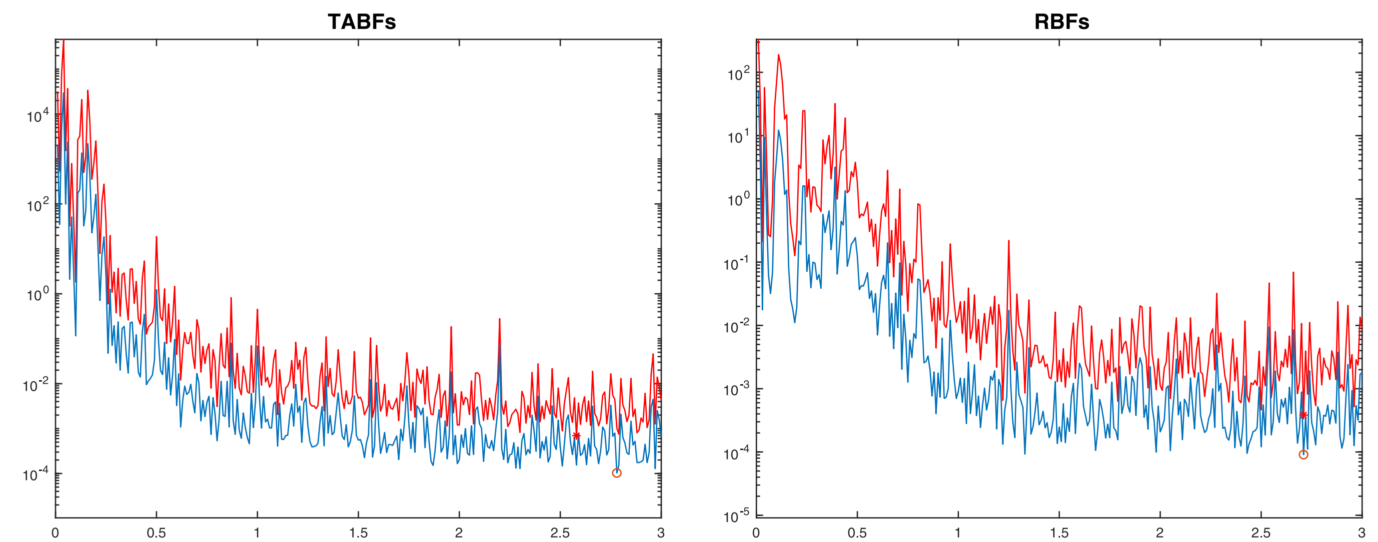

Fig. 15. Maximum error (Red) and RMSE (Blue) when distribution 4 is used. (For interpretation of the references to color in this figure legend, the reader is referred to the web version of this article).

The collocation points are equally distributed on $\partial\Omega$. As for the selection of source points, we use four different distributions which are given in Fig. 11. We use $M = 1070$ testing points for calculating the error. We compute numerical solutions of MFS and MTABF on these four types of source points. Distributions 2 and 3 are more regular than the other two distributions. Numerical results presented in Figs. 12–15 and Table 8 show that the best numerical approximation is obtained when distribution 2 is used.

The comparison also demonstrates that numerical approximations of MFS and MTABF are comparable on each type of source points.

5. Concluding remarks

In this paper, we propose an approach to improve the method of angular basis functions that was investigated in [17]. As pointed out in [17], MABF has some limitations on the selection of source points because the range of angular basis function θ should be restricted to $(-\pi/2, \pi/2)$, otherwise it will cause ill conditioning of the coefficient matrix. The proposed method transforms all values of θ associated with each source point to the interval $(-\pi/2, \pi/2)$. Meanwhile, each transformed angular basis function $\bar{\theta}$ is still a fundamental solution of the Laplace equation. As a consequence, there is no need to specially design a source point distribution for $\bar{\theta}$. Therefore, The proposed method (i.e. MTABF) can directly adopt source point distributions used in traditional MFS. The effort in seeking proper location of source points for MABF is then significantly reduced.

Acknowledgments

The authors thank the anonymous referees for their critical and constructive comments which improved the presentation and the quality of this paper. The first author was partially supported by the National Natural Science Foundation of China (Grant no. 11201288). The third author was partially supported by the National Multiple Sclerosis Society (Grant no. RG5265 A1), BrightFocus Foundation (Grant no. A2017330S), NIH/National Institute on Aging (Grant no. R01AG053548), NIH/National Institute of Child Health and Human Development (Grant no. R01HD094381).

References

[1] Aoki Y. Analysis of asymptotic solutions for cusp problems in capillarity. Department of Applied Mathematics, University of Waterloo; 2007. M.S. thesis.
[2] Baker JM, Nieber JL. An analysis of the steady-state heat balance method for measuring sap flow in plants. Agric For Meteorol 1989;48(12):93–109.
[3] Chen JT, Chou KH, Lee YT. A novel method for solving the displacement and stress fields of an infinite domain with circular holes and/or inclusions subject to a screw dislocation. Acta Mech 2011;218(115132).
[4] Cho HA, Golberg MA, Muleshkov AS, Li X. Trefftz methods for time dependent partial differential equations. CMC: Comput Mater Contin 2004;1:1–37.
[5] Cruse TA, Ewing AP, Wikswo JP. Green's function formulation of laplace's equation for electromagnetic crack detection. Comput Mech 1999;23(420429).
[6] Fairweather G, Karageorghis A. The method of fundamental solutions for elliptic boundary value problems. Adv Comput Math 1998;9:69–95.
[7] Fairweather G, Karageorghis A, Martin PA. The method of fundamental solutions for scattering and radiation problems. Eng Anal Bound Elem 2003;27:759–69.
[8] Fearn RL. Airfoil aerodynamics using panel methods. Math J 2008:725739.
[9] Golberg MA, Chen CS. The method of fundamental solutions for potential Helmholtz and diffusion problems. In: Golberg MA, editor. Boundary integral methods: numerical and mathematical aspects. Boston: WIT Press and Computational Mechanics Publications; 1999. p. 105–76.
[10] Kuethe AM., Chow CY.. Foundations of aerodynamics: bases of aerodynamic design. 4th ed.John Wiley & Sons, Inc.1986.
[11] Kupradze VD, Aleksidze MA. The method of functional equations for the approximate solution of certain boundary value problems. USSR Comput Math Math Phys 1964;4:82–126.
[12] Lewis RI. Vortex element methods for fluid dynamic analysis of engineering systems. Fluid mechanics and heat transfer. Cambridge University Press; 1991.
[13] Li M, Chen CS, Karageorghis A. The MFS for the solution of harmonic boundary value problems with non-harmonic boundary conditions. Comput Math Appl 2013;66(11):2400–24.
[14] Lv H, Hao F, Wang Y, Chen CS. The MFS versus the Trefftz method for the laplace equation in 3d. Eng Anal Bound Elem 2017;83:133–40.
[15] Mathon R, Johnston RL. The approximate solution of elliptic boundary value problems by fundamental solutions. SIAM J Numer Anal 1977;14:638–50.
[16] Phillips W.F.. Mechanics of flight. John Wiley & Sons, Inc.; 2004.
[17] Young DL, Huang YJ, Wu CS, Sladek V, Sladek J. Angular basis functions formulation for 2d potential flows with non-smooth boundaries. Eng Anal Bound Elem 2015;61:1–15.